NASA TN D-995

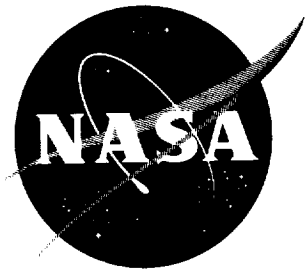

TECHNICAL NOTE

D-995

AERODYNAMIC LOADS ON AN ISOLATED SHROUDED-PROPELLER CONFIGURATION FOR ANGLES OF ATTACK FROM -10° TO 110°

By Kalman J. Grunwald and Kenneth W. Goodson

Langley Research Center
Langley Air Force Base, Va.

NATIONAL AERONAUTICS AND SPACE ADMINISTRATION
WASHINGTON
January 1962

NATIONAL AERONAUTICS AND SPACE ADMINISTRATION

TECHNICAL NOTE D-995

AERODYNAMIC LOADS ON AN ISOLATED SHROUDED-PROPELLER CONFIGURATION FOR ANGLES OF ATTACK FROM -10° TO 110°

By Kalman J. Grunwald and Kenneth W. Goodson

SUMMARY

An investigation of the division of loads between the propeller and the shroud of a shrouded-propeller configuration was conducted in the 17-foot test section of the Langley 300-MPH 7- by 10-foot tunnel. This investigation covered an angle-of-attack range from -10° to 110° and a range of advance ratios (0 to 0.595) typical of the transition speed range of a tilt-duct VTOL aircraft.

For the configurations with fixed blade angle (24° at the three-quarter radius), the normal force and pitching moment developed by the propeller and spinner were only a relatively small part of the overall normal force and pitching moment of either a stalled or an unstalled shroud. The ratio of the thrust of the propeller and spinner to total thrust was found to vary from about 0.4 in hovering to about 0.7 at the highest advance ratio of the tests, 0.595, with the shroud at zero angle of attack.

INTRODUCTION

The ducted- or shrouded-propeller configuration has been proposed as one means of attaining VTOL flight. At the present time information is available on the aerodynamic performance of wing-tip-mounted tiltable shrouded-propeller configurations. (For example, see refs. 1 to 3.) Information on the division of loads between the shroud and the propeller is useful in analyzing aerodynamic performance and structural requirements. Because of the scarcity of such information, the present program has been conducted to obtain experimental data on the division of loads for an isolated shrouded-propeller configuration.

The basic shrouded propeller of this investigation was previously used (mounted on a wing tip) in the investigation reported in reference 1. The shroud had 5/16 the dimensions of the shrouded-propeller configuration

of reference 2 but the propeller design was different. The results in reference 1 showed that, because of the low Reynolds numbers of the tests, the stalling characteristics of the smaller shroud differed from those of the larger shroud of reference 2. Therefore the basic configuration was modified by the addition of shroud leading-edge fairings to alleviate this shortcoming. Inasmuch as the range of Reynolds numbers of the present tests is the same as that in reference 1, both the basic model and the modified model (which incorporated the smaller of the leading-edge fairings used in ref. 1) were employed in the present investigation. The models were tested through an angle-of-attack range from -10° to 110°. The advance ratio was varied from 0 to 0.595. The propeller-blade angle at the three-quarter radius was held constant at 24°. Tests were conducted in the 17-foot test section of the Langley 300-MPH 7- by 10-foot tunnel (ref. 4). L 1 6 1 7

Presented herein, for both the basic and modified configurations, are measured force and moment coefficients of the shroud without a propeller, the shroud with a windmilling propeller, and the shroud with a thrusting propeller. Included in the last category are measurements of force and moment coefficients of the propeller and spinner operating within the shroud.

SYMBOLS

b	propeller-blade section chord, ft
c	duct chord, 0.859 ft
C_L	lift coefficient, L/qS
C_m	pitching-moment coefficient, M/qSc
C_Q	torque coefficient, $Q/\rho n^2 D^5$
C_T	thrust coefficient, $T_p/\rho n^2 D^4$
C_X	longitudinal-force coefficient, F_X/qS
D	propeller diameter, 1.25 ft
F_X	longitudinal force, lb
h	propeller blade-section thickness, ft
L	lift, lb

M	total pitching moment, ft-lb
M_p	propeller pitching moment, ft-lb
n	propeller rotational speed, rps
N	total normal force, lb
N_p	propeller normal force, lb
q	dynamic pressure, $\frac{1}{2}\rho V^2$
Q	motor shaft torque, ft-lb
r	radius to propeller blade element, ft
R	propeller-tip radius, ft
S	projected shroud area, (Shroud chord) × (Exit diameter), 1.21 sq ft
T	total thrust, lb
T_o	hovering thrust, 45 lb
T_p	propeller thrust (including spinner forces), lb
V	free-stream velocity, ft/sec
x	transfer distance from propeller-moment reference point to duct-moment reference point, 0.125 ft
α	angle of attack, deg
β	blade-section angle, deg
$\beta_{.75}$	blade angle at three-quarter radius
η	net efficiency, $TV/2\pi Qn$
ρ	density, slugs/cu ft

MODELS AND APPARATUS

Photographs of the basic symmetrical model are shown in figure 1. A side-view sketch giving the principal dimensions and showing the major features of the model support system is presented in figure 2. Basic shroud coordinates are given in table I. The leading-edge fairing employed to adjust the shroud-stalling characteristics of the model is outlined in figure 3. Because of its purpose, no great attention is given to details of the fairing.

The three-blade propeller was constructed of plastic reinforced with glass fiber over a balsa-wood core. Geometric characteristics of the propeller blade are given in figure 4. Blade sections consisted of NACA 6412 airfoil sections. The blade-angle setting at the three-quarter radius was 24°. The shrouded propeller had a tip clearance of 0.04 inch and a root clearance of 0.10 inch.

The model was supported in the tunnel by a shielded sting-support system attached at the rear of the motor nacelle as indicated in figure 2. Total forces and moments were measured with a three-component strain-gage balance located at the foot of the strut. Forces and moments of the combined propeller and spinner were measured with strain-gage beams mounted within the motor nacelle. The thrust of the combined propeller and spinner T_p was measured as shaft tension without corrections for pressure differences within the nacelle. Such corrections in the present case are believed to be very small.

TESTS

Measurements of the forces and moments of the shrouds with the propeller removed and with a windmilling propeller were made at a tunnel speed of 100 feet per second. Powered tests, with a constant propeller rotational speed of 8,000 rpm, were made at the various tunnel speeds required to cover the desired range of advance ratio V/nD. At each selected advance ratio, the angle of attack was varied over a range which would include anticipated conditions of steady level flight, climb, and descent for tilt-duct VTOL configurations. Measurement of the thrust defined herein as hovering thrust T_o was made at $\alpha = 90°$; in view of the large ratio of the volume of the surrounding enclosure to the volume of flow through the shroud, the effect of the surrounding enclosure on the measured hovering thrust is believed to be extremely small.

Since power-off tests were made at a wind speed of 100 feet per second, the Reynolds number based on shroud chord was 550,000. For the

power-on tests, the Reynolds number varied from 0 at $V/nD = 0$ to 550,000 at $V/nD = 0.595$ (the maximum V/nD of the tests).

DATA REDUCTION

The results are referred to the system of wind axes shown in figure 5. Locations of the shroud pitching-moment axis and propeller pitching-moment axis are given in figure 2.

The free-stream dynamic pressure was used in nondimensionalizing the data for the power-off conditions and the data in the relatively high-speed flight regime. However, in the transition speed range, coefficients based on the free-stream velocity would approach infinite values near hovering flight; to avoid this problem, transition speed-range data have been nondimensionalized by dividing by the static thrust in hovering.

RESULTS AND DISCUSSION

The basic data for the shroud configuration with the lip modification are presented in figures 6 and 7. Figures 8 and 9 contain the basic data for the unmodified configuration. Figures 6 and 8, which contain the data for the highest speed condition tested, show the results for conditions of power off with propellers off, power off with propellers windmilling, and power on with propellers operating at $V/nD = 0.595$.

Power-Off Characteristics

In the plots of figures 6 and 8 for lift coefficient as a function of longitudinal force coefficient, it can be observed that the maximum lift coefficient of the shroud with a windmilling propeller is greater than that of the shroud with the propeller removed. This higher lift is attributed to the action of the propeller in redistributing flow energy through the duct, to the lift component of the propeller, and to a delay of flow separation within the duct due to the turbulent action of the propeller-blade wake on the duct boundary layer; and of course there may be other causes. Redistribution of flow energy in the duct arises from the action of the propeller in removing energy from regions of high velocity and adding energy to regions of low velocity in the duct.

Power-On Characteristics

The basic data obtained through the angle-of-attack and advance-ratio ranges of the tests are presented in figures 7 and 9 for the modified and unmodified configurations, respectively. As mentioned earlier, the low Reynolds numbers of the tests gave rise to a region of stalled operation in the case of the unmodified shroud. Tuft studies made during the tests gave evidence that the stall was due to flow separation from the shroud lip; the occurrence of stall was marked by a distinct change in the character of the noise emitted by the model. In figure 9 the stall is marked by rapid reductions in the lift and pitching-moment curves and by sharp increases in thrust and torque. For the modified configuration (fig. 7) the rapid changes do not occur. Up to the point of lip stall, the characteristics for the unmodified configuration are practically the same as those for the modified configuration.

L 1 6 1 7

Division of Loads

The primary purpose of this investigation was to determine the division of aerodynamic loads between the shroud and the propeller.

The results in figure 7(c) (modified configuration) and figure 9(c) (unmodified configuration) show that the propeller contribution to the overall normal force and pitching moment of either configuration is relatively small. Relative magnitudes are shown more directly in figures 10 and 11. Although stalled operation (fig. 9(c)) causes appreciable changes in propeller normal-force and pitching-moment characteristics, these quantities remain small in comparison with the overall values.

The ratio of propeller thrust to total thrust as a function of angle of attack for a number of advance ratios is shown in both configurations in figure 12. In hovering ($V/nD = 0$), the propeller carries approximately 40 percent of the total thrust. At the highest V/nD value of the tests, 0.595, the propeller carries about 70 percent when α is near 0°.

For the unstalled operation, figure 12(a), the ratio of propeller thrust to total thrust generally decreases as α increases at a constant value of V/nD. Beyond the stall, on the other hand, the ratio increases as α increases (fig. 12(b)). This increase in thrust ratio is due primarily to a reduction in shroud thrust caused by the lip stall (fig. 9(c)), and is due partly to an increase in propeller thrust which is also caused by the lip stall (fig. 9(b) or 9(c)).

In figure 13, the propulsive efficiency and thrust ratio obtained for the modified configuration at $\alpha = 0^\circ$ and $V/nD = 0.595$ are shown, together with curves obtained from reference 5 (a sharp-radius inlet configuration). From the position of the propulsive-efficiency point

of the present configuration in relation to the efficiency curves of the reference configuration, it can be judged that peak efficiency was not reached with the present configuration; it occurs at a value of V/nD higher than 0.595. For the reference configuration the thrust ratio lies in the neighborhood of 0.9 at V/nD = 0.595, and the result for the present investigation is 0.7. Some of this difference is due to the difference in the ratio of shroud-exit diameter to propeller diameter for the two configurations.

SUMMARY OF RESULTS

For the shrouded-propeller configuration of the present investigation the normal force and pitching moment developed by the propeller and spinner are a relatively small part of the overall normal force and pitching moment of either a stalled or an unstalled shroud; therefore, the duct is the primary source of pitching moment and normal force loads.

The ratio of the thrust of the propeller and the spinner to the total thrust varies from about 0.4 in hovering to about 0.7 at the highest advance ratio of the tests, 0.595, with the shroud at zero angle of attack. For the unstalled operation this thrust ratio in general decreases as angle of attack increases at constant advance ratio. Beyond the stall and at constant advance ratio, on the other hand, the thrust ratio increases when the angle of attack increases.

Langley Research Center,
National Aeronautics and Space Administration,
Langley Air Force Base, Va., September 28, 1961.

REFERENCES

1. Goodson, Kenneth W., and Grunwald, Kalman J.: Aerodynamic Characteristics of a Powered Semispan Tilting-Shrouded-Propeller VTOL Model in Hovering and Transition Flight. NASA TN D-981, 1962.

2. Yaggy, Paul F., and Mort, Kenneth W.: A Wind-Tunnel Investigation of a 4-Foot-Diameter Ducted Fan Mounted on the Tip of a Semispan Wing. NASA TN D-776, 1961.

3. Tapscott, Robert J., and Kelley, Henry L.: A Flight Study of the Conversion Maneuver of a Tilt-Duct VTOL Aircraft. NASA TN D-372, 1960.

4. Kuhn, Richard E., and Hayes, William C., Jr.: Wind-Tunnel Investigation of Longitudinal Aerodynamic Characteristics of Three Propeller-Driven VTOL Configurations in the Transition Speed Range, Including Effects of Ground Proximity. NASA TN D-55, 1960.

5. Grose, Ronald M.: Wind Tunnel Tests of Shrouded Propellers at Mach Numbers From 0 to 0.60. WADC Tech. Rep. 58-604, ASTIA Doc. No. AD-205464, U.S. Air Force, Dec. 1958.

TABLE I.- DUCT COORDINATES

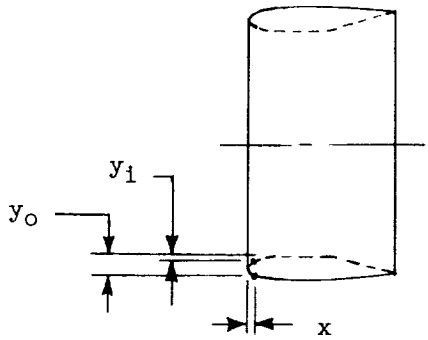

x, in.	y_i, in.	y_o, in.
0	0.875	0.875
.078	.663	1.144
.125	.589	1.206
.188	.513	1.256
.250	.463	1.287
.312	.406	1.325
.438	.337	1.375
.625	.263	1.437
.938	.163	1.506
1.250	.100	1.556
1.562	.050	1.587
1.875	.019	1.613
2.188	.006	1.625
2.500	0	1.637
2.812	0	1.644
Straight line	0	1.644
↓	0	1.644
	0	1.644
	0	1.644
	0	1.644
	0	1.644
5.375	0	1.644
5.938	Straight line	1.625
6.250	↓	1.600
6.562		1.575
6.875		1.537
7.188		1.500
7.500		1.463
7.812		1.425
8.125		1.375
8.438		1.331
8.750		1.281
9.375	↓	1.163
10.312	.950	.981

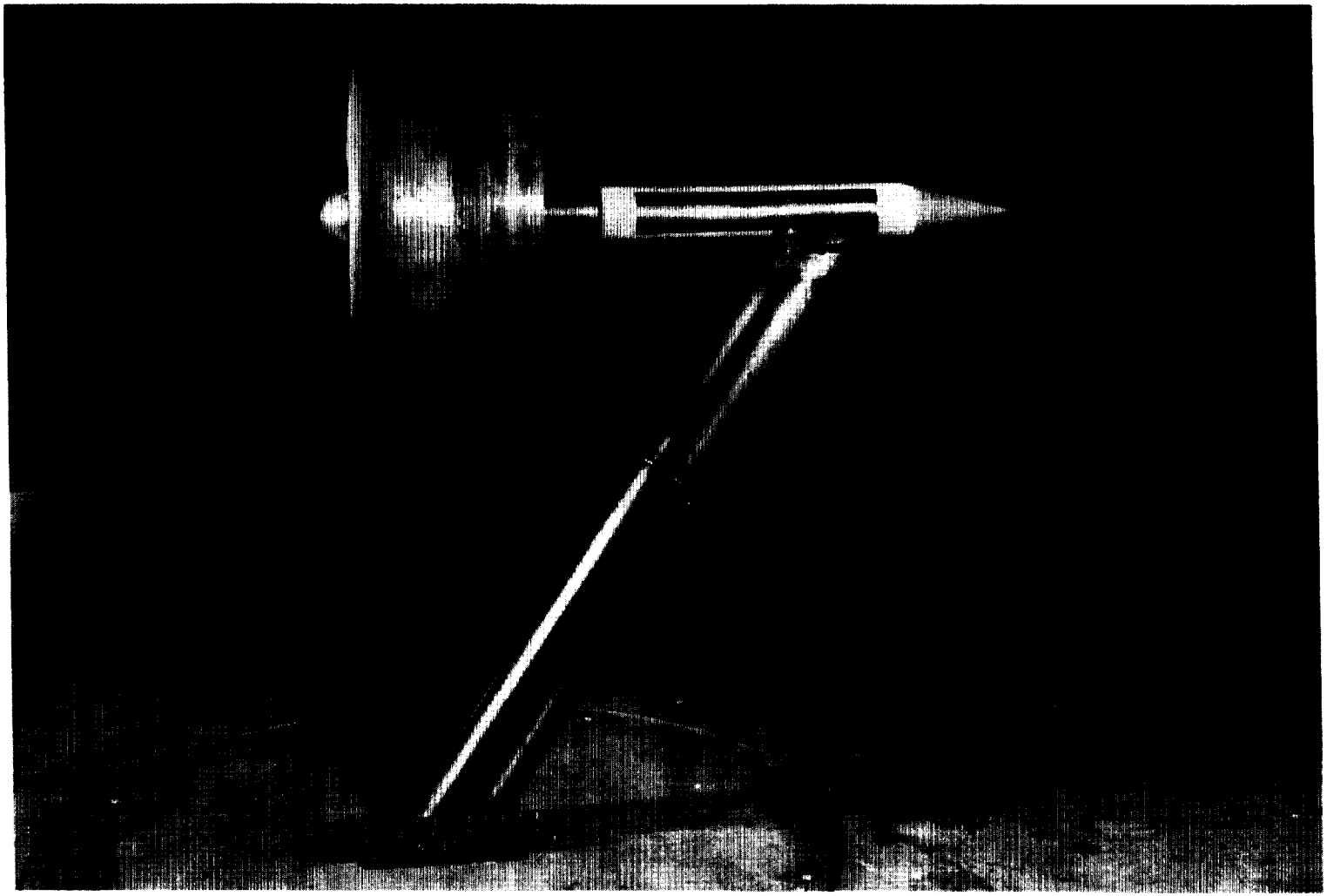

Figure 1.- Photograph of model. L-60-541

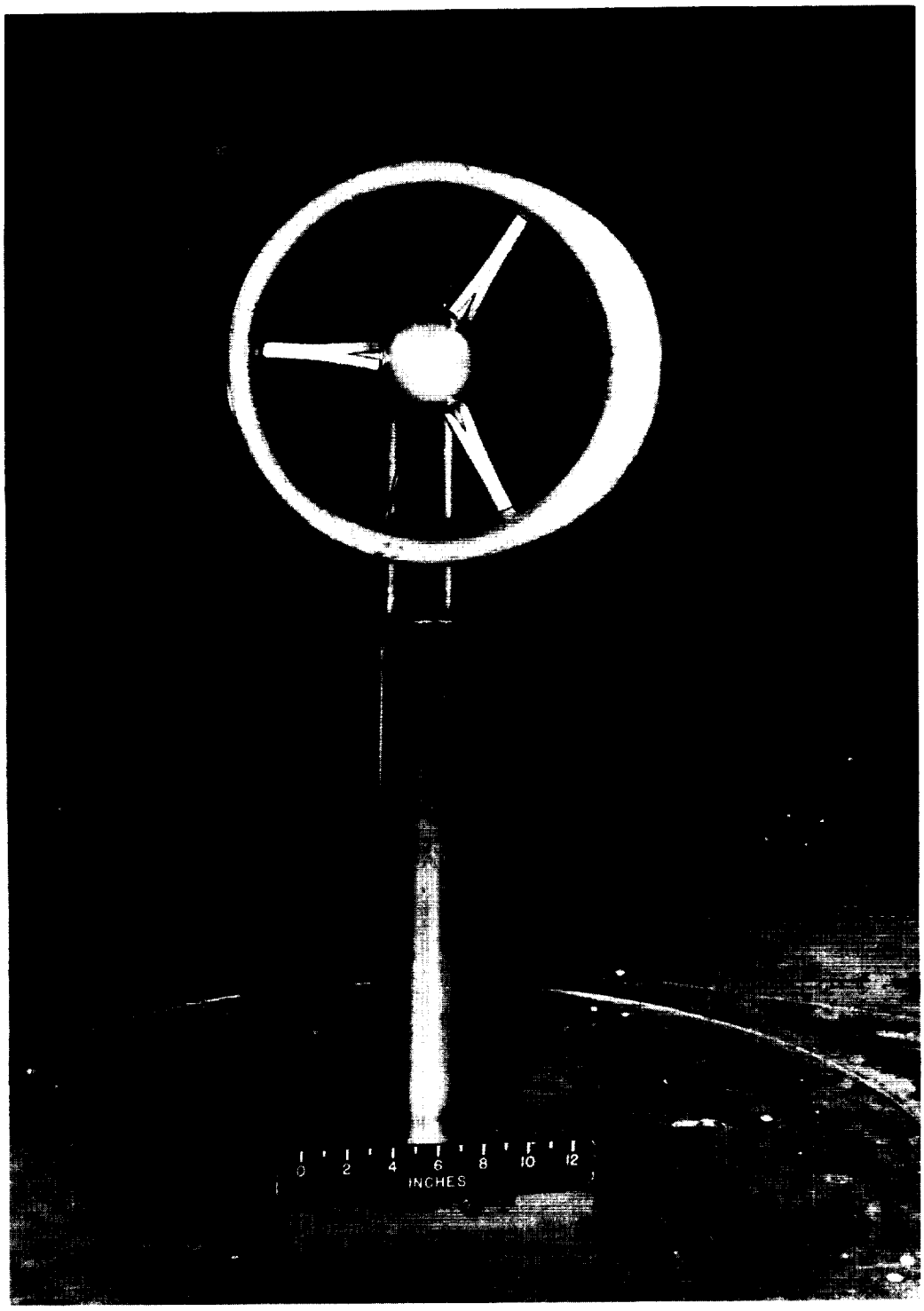

Figure 1.- Concluded. L-60-543

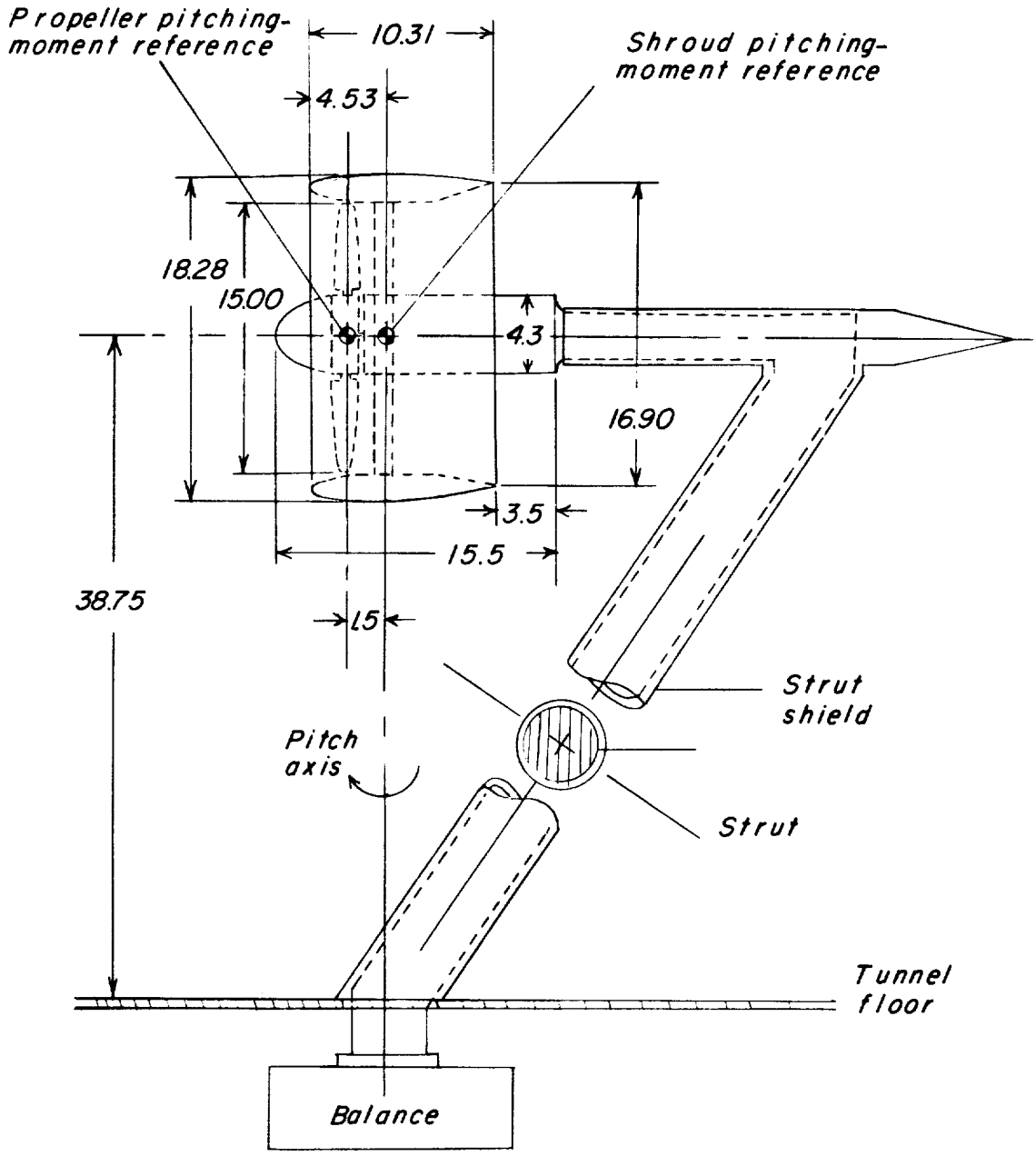

Figure 2.- Sketch of model and model support system. Dimensions are in inches.

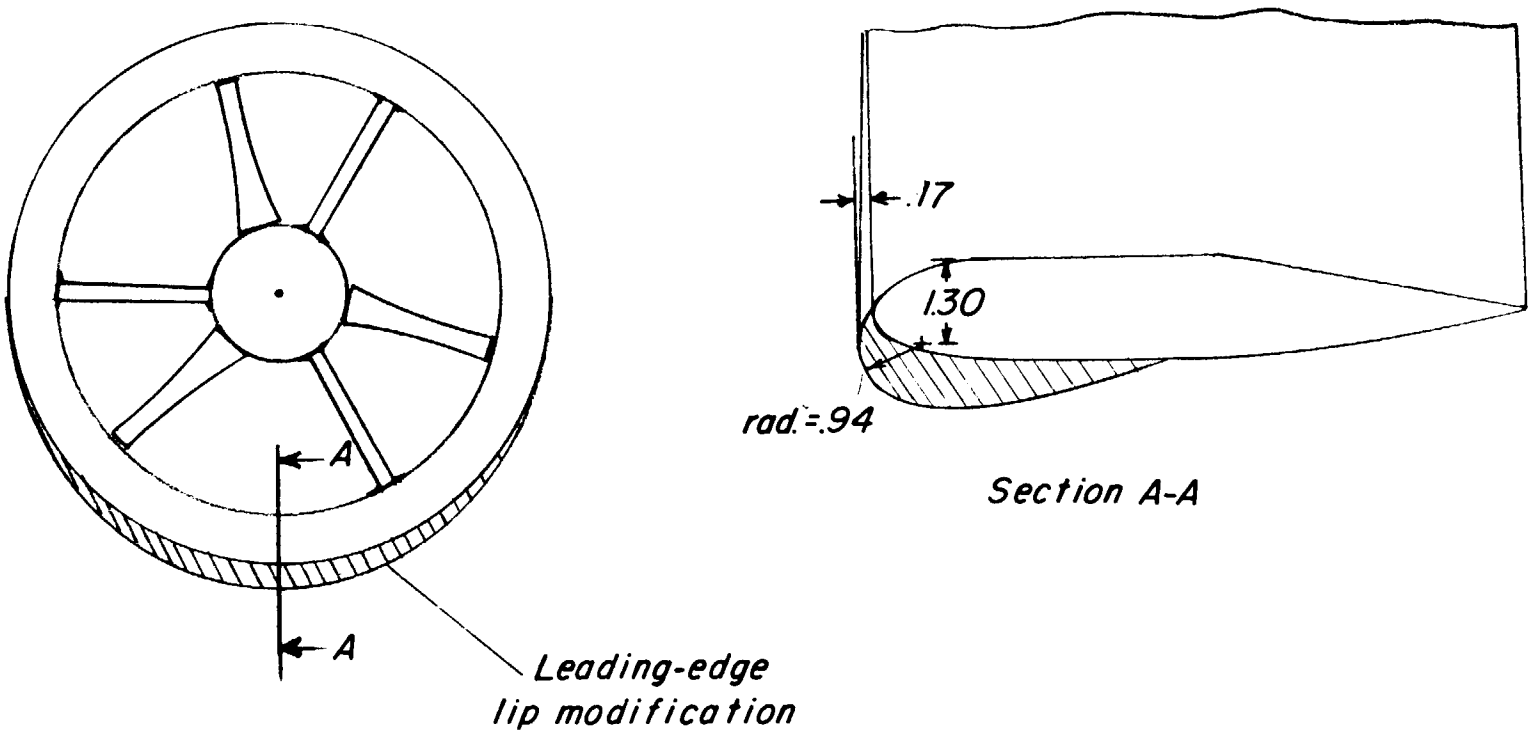

Figure 3.- Drawing of duct with leading-edge-lip modification.

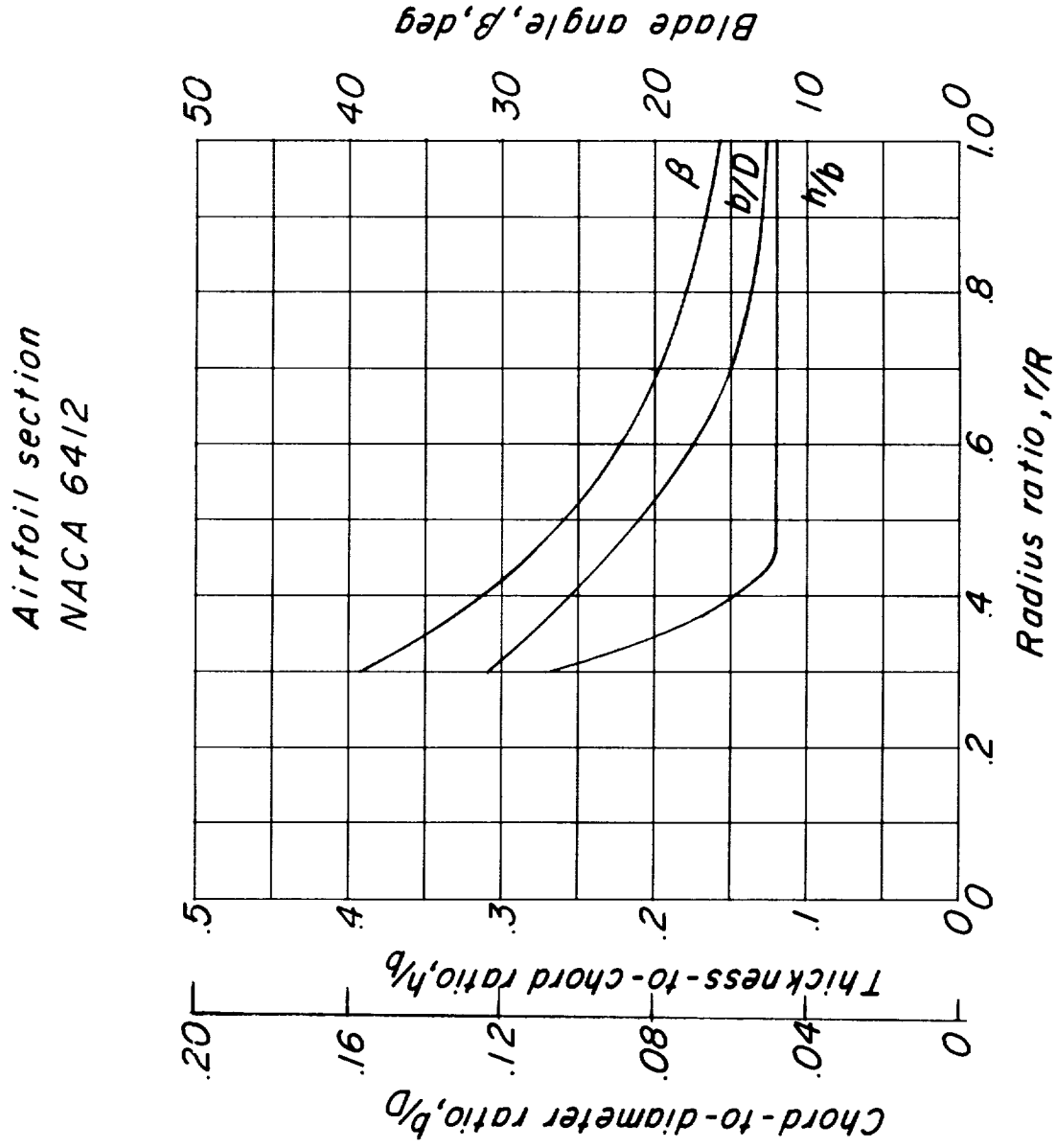

Figure 4.- Propeller-blade geometric characteristics.

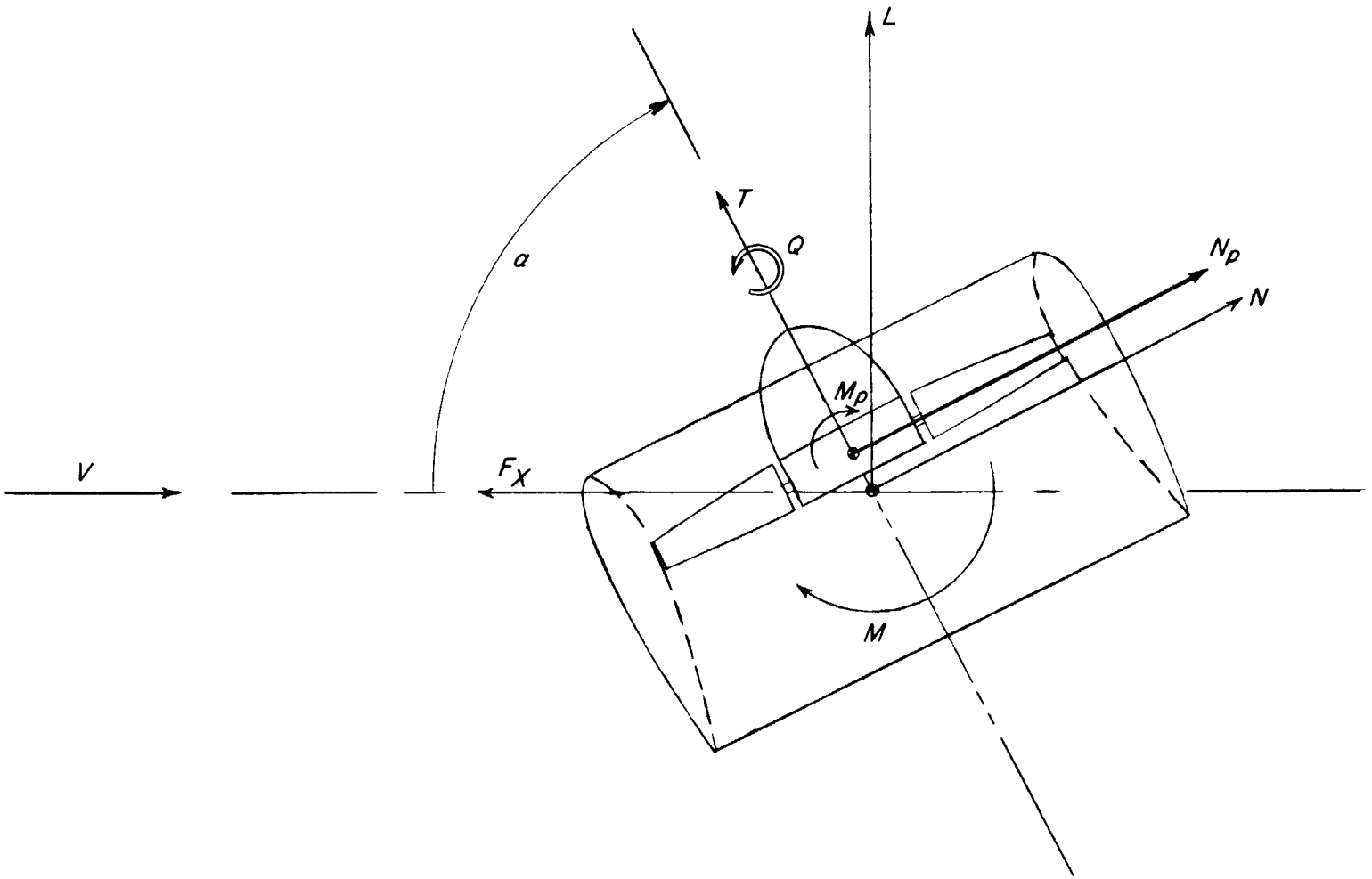

Figure 5.- System of axes used, showing positive sense of forces, moments, angles, and velocity.

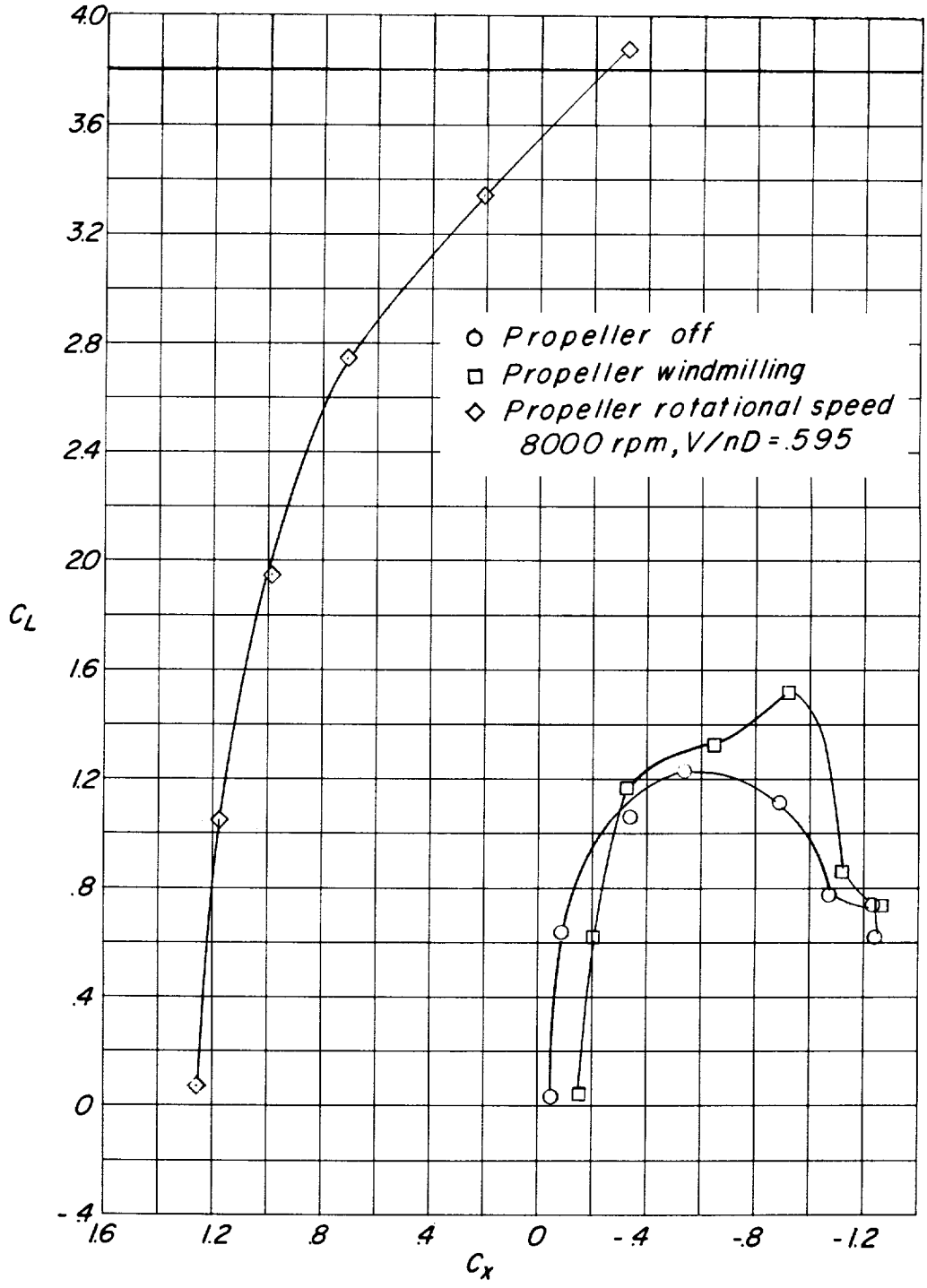

L-1617

Figure 6.- Aerodynamic characteristics of the modified-lip configuration in the power-off and low-power condition.

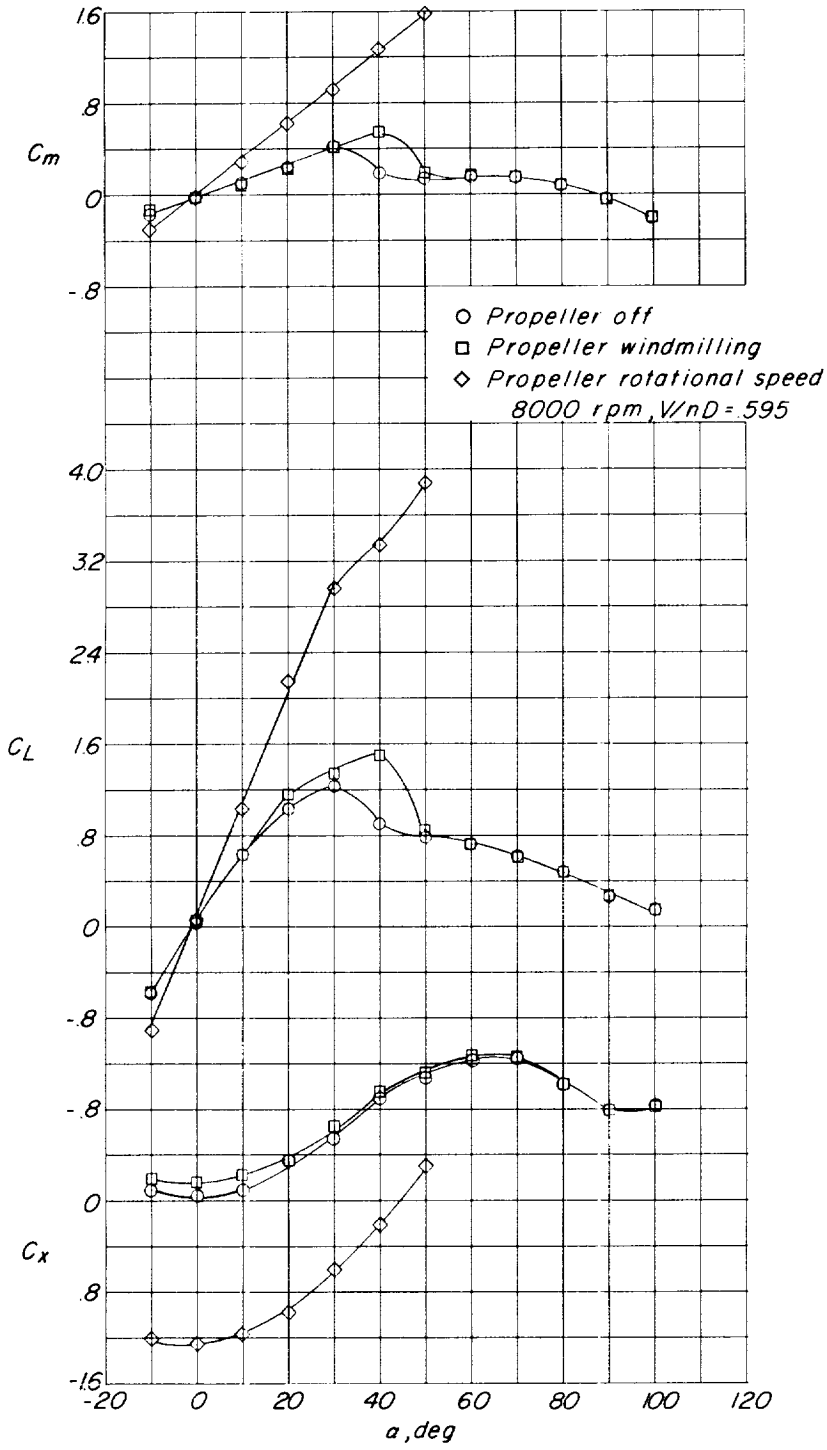

Figure 6.- Concluded.

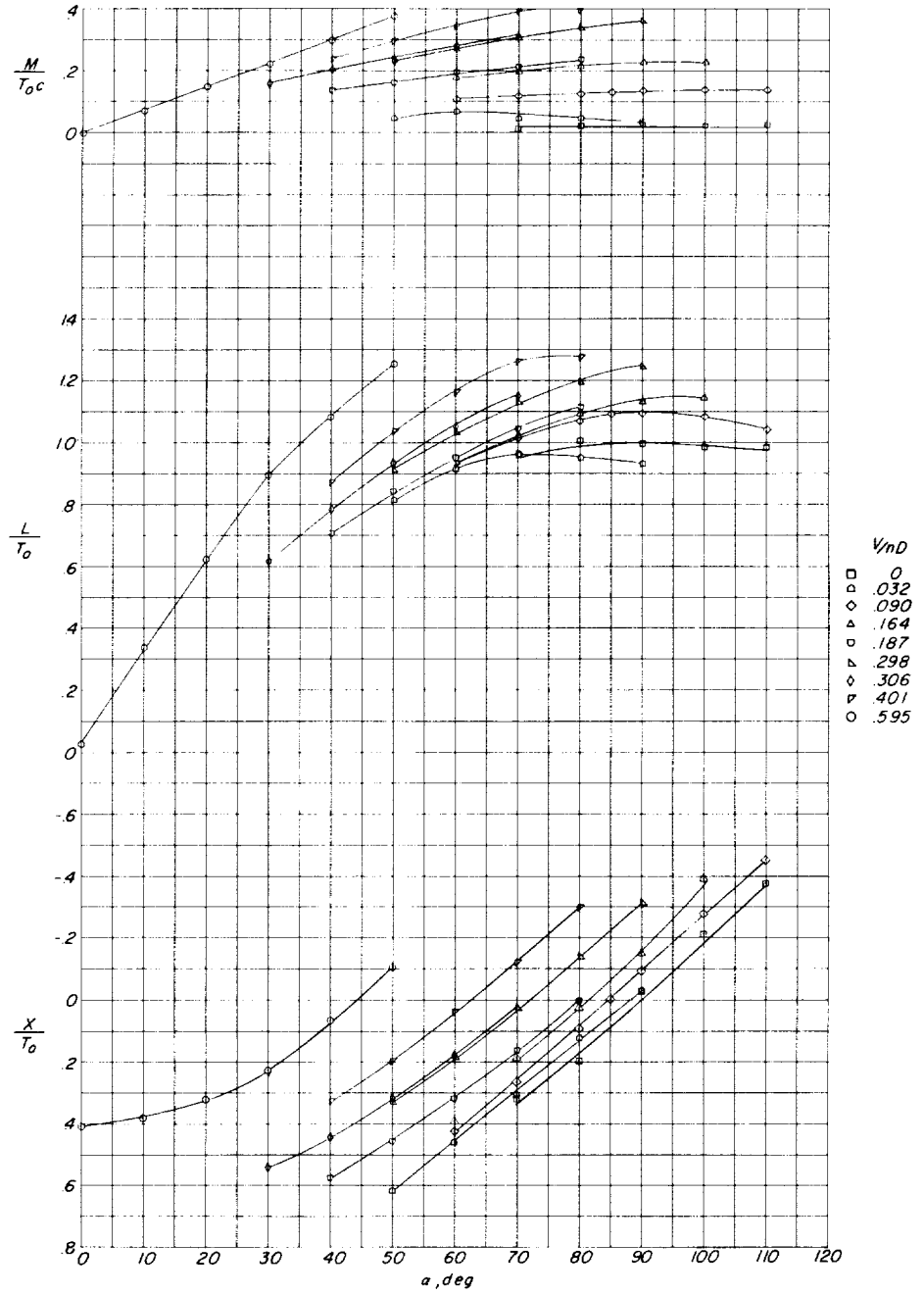

(a) Lift, longitudinal force, and pitching moment (modified-lip configuration).

Figure 7.- Effect of advance ratio and angle of attack on the aerodynamic characteristics of the modified-lip configuration.

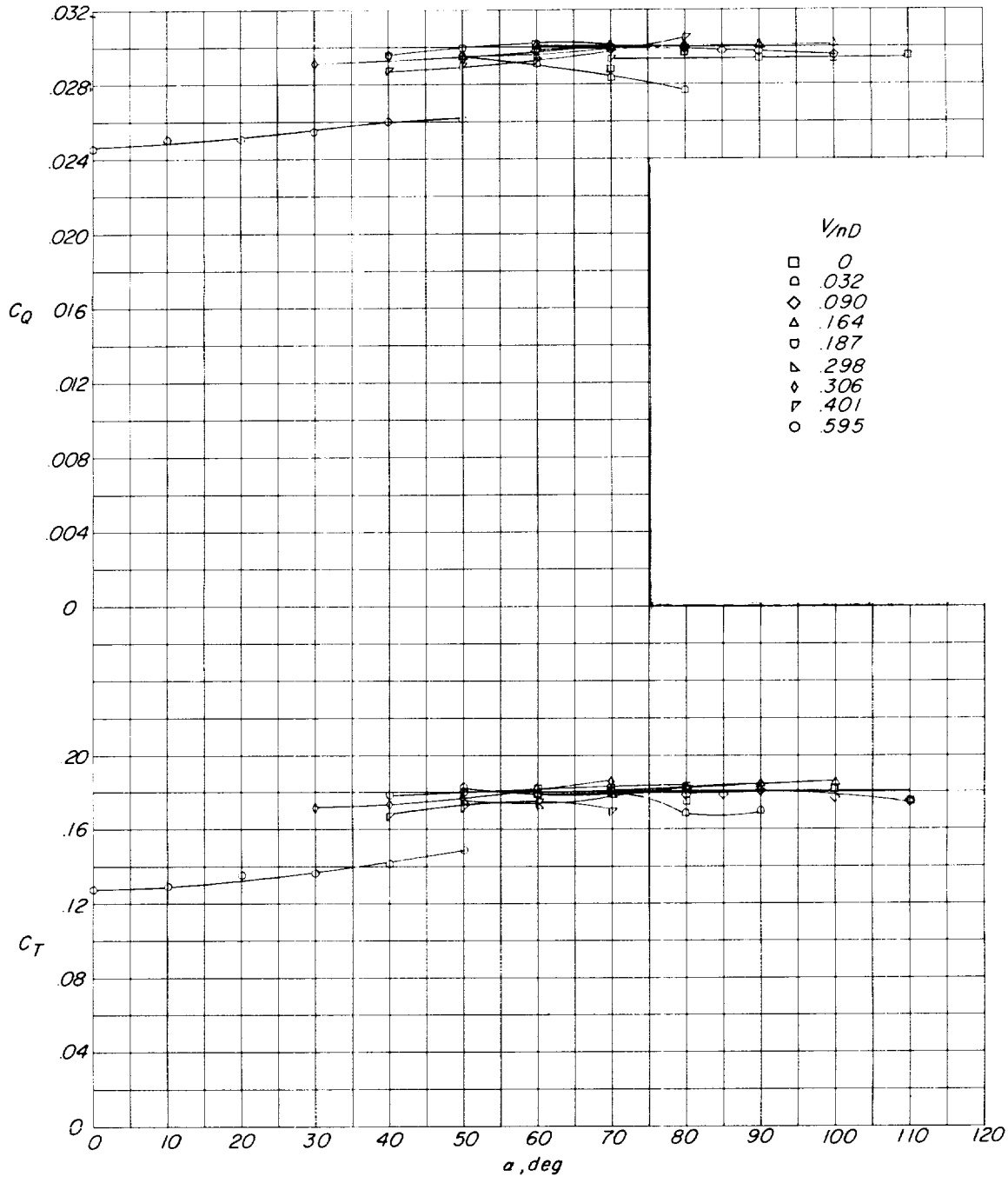

(b) Propeller thrust and torque coefficients (modified-lip configuration).

Figure 7.- Continued.

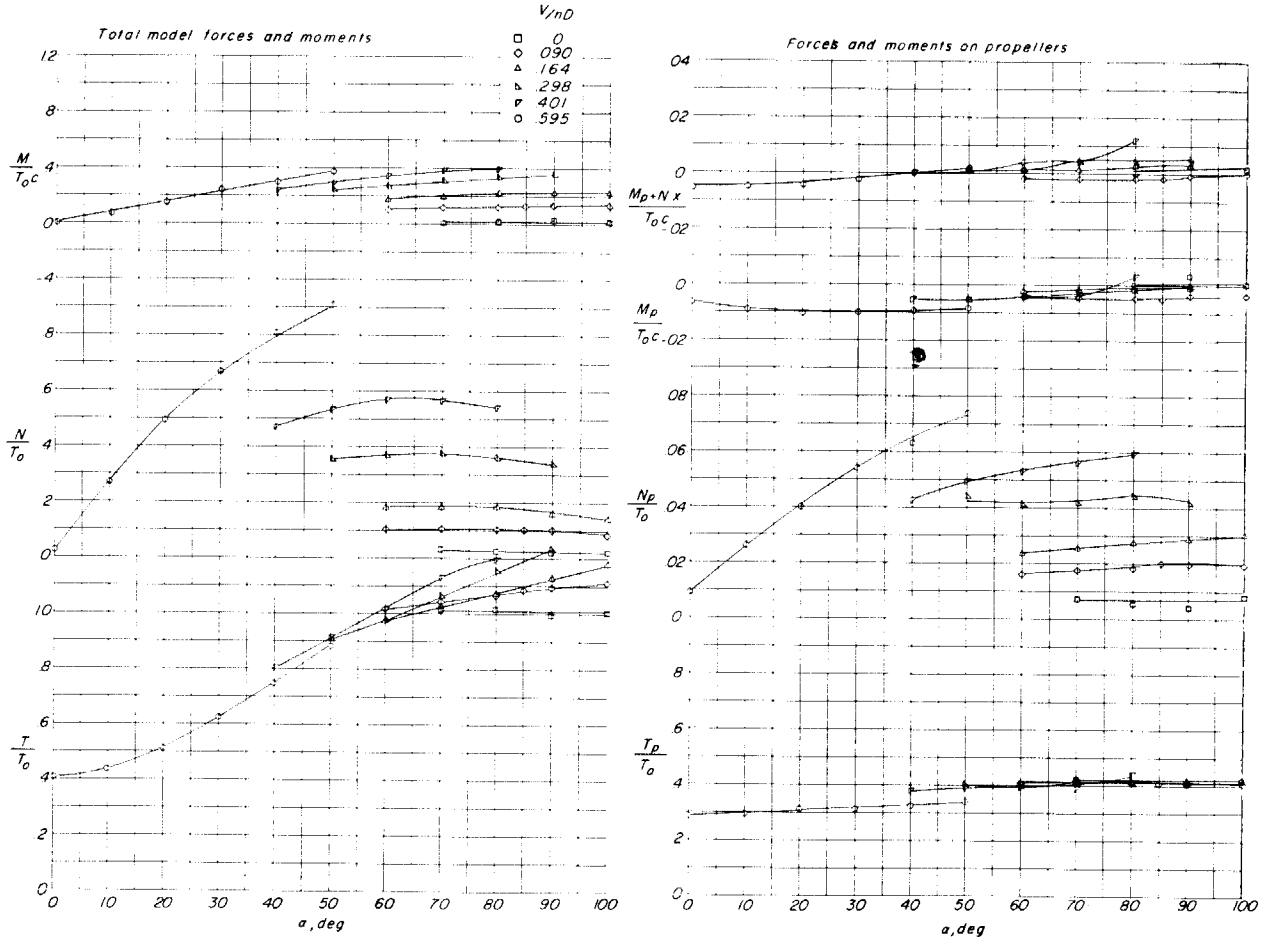

(c) Comparison of the forces and moments on the propeller with the total model forces (modified-lip configuration).

Figure 7.- Concluded.

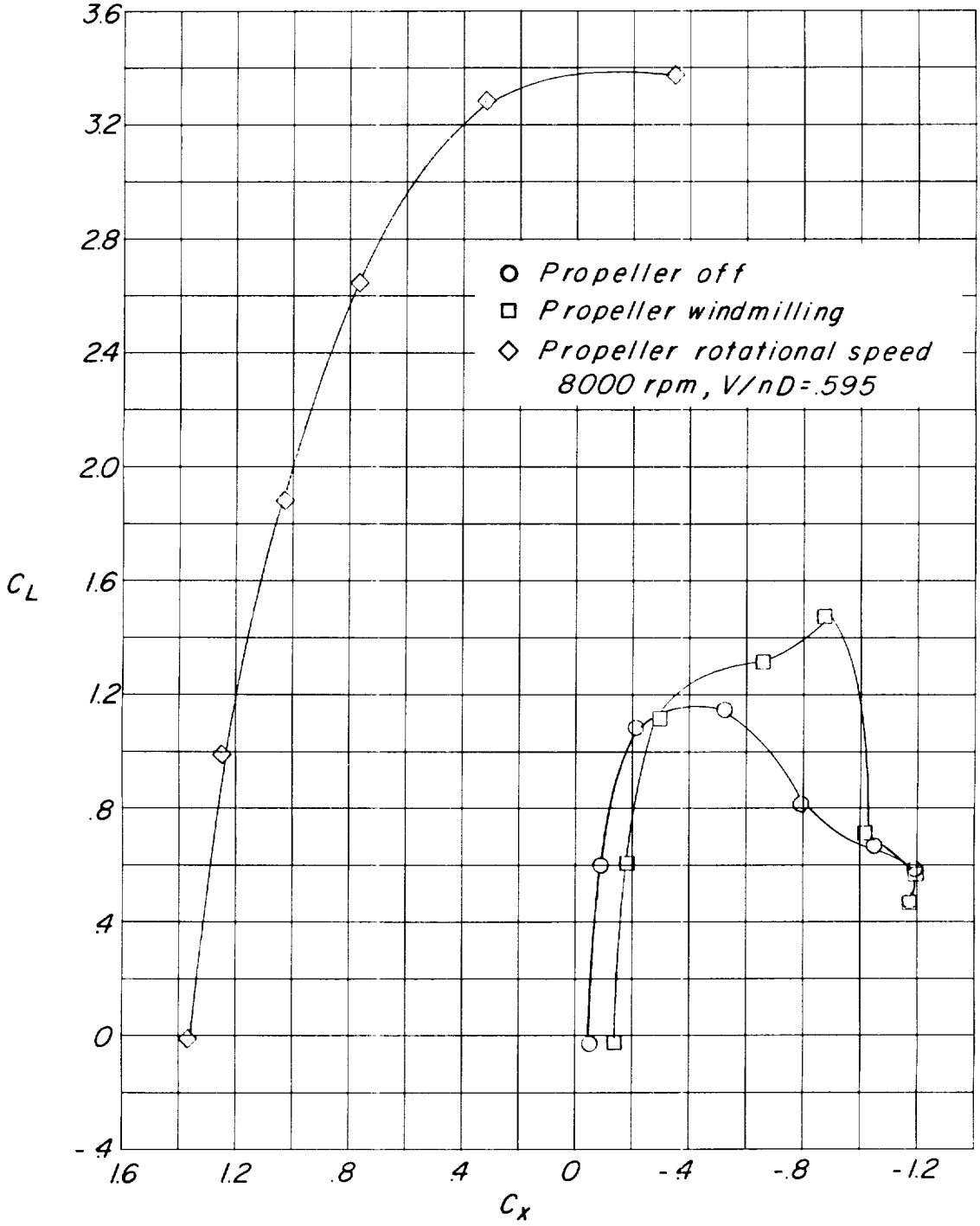

Figure 8.- Aerodynamic characteristics of the original-lip configuration in the power-off and low-power condition.

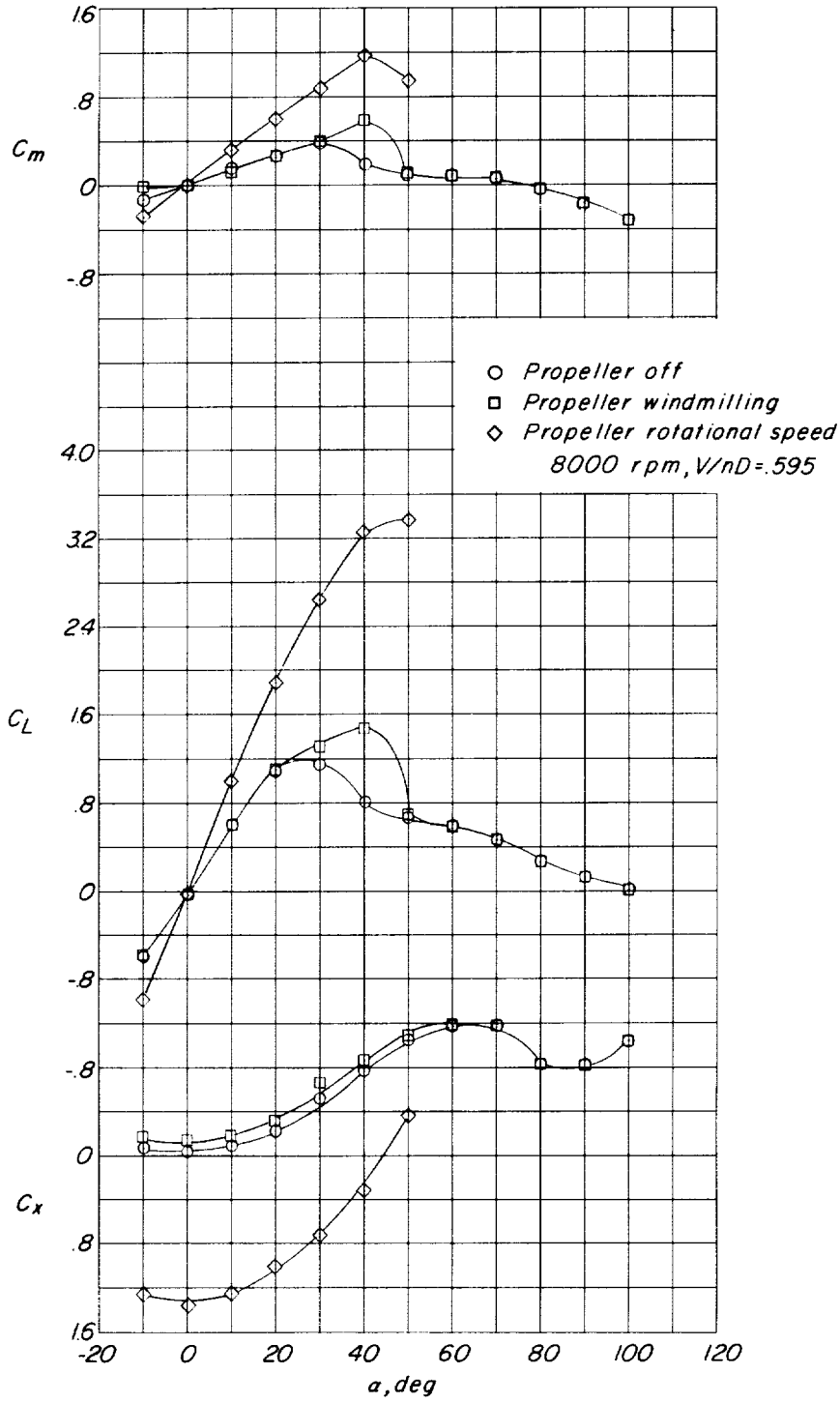

Figure 8.- Concluded.

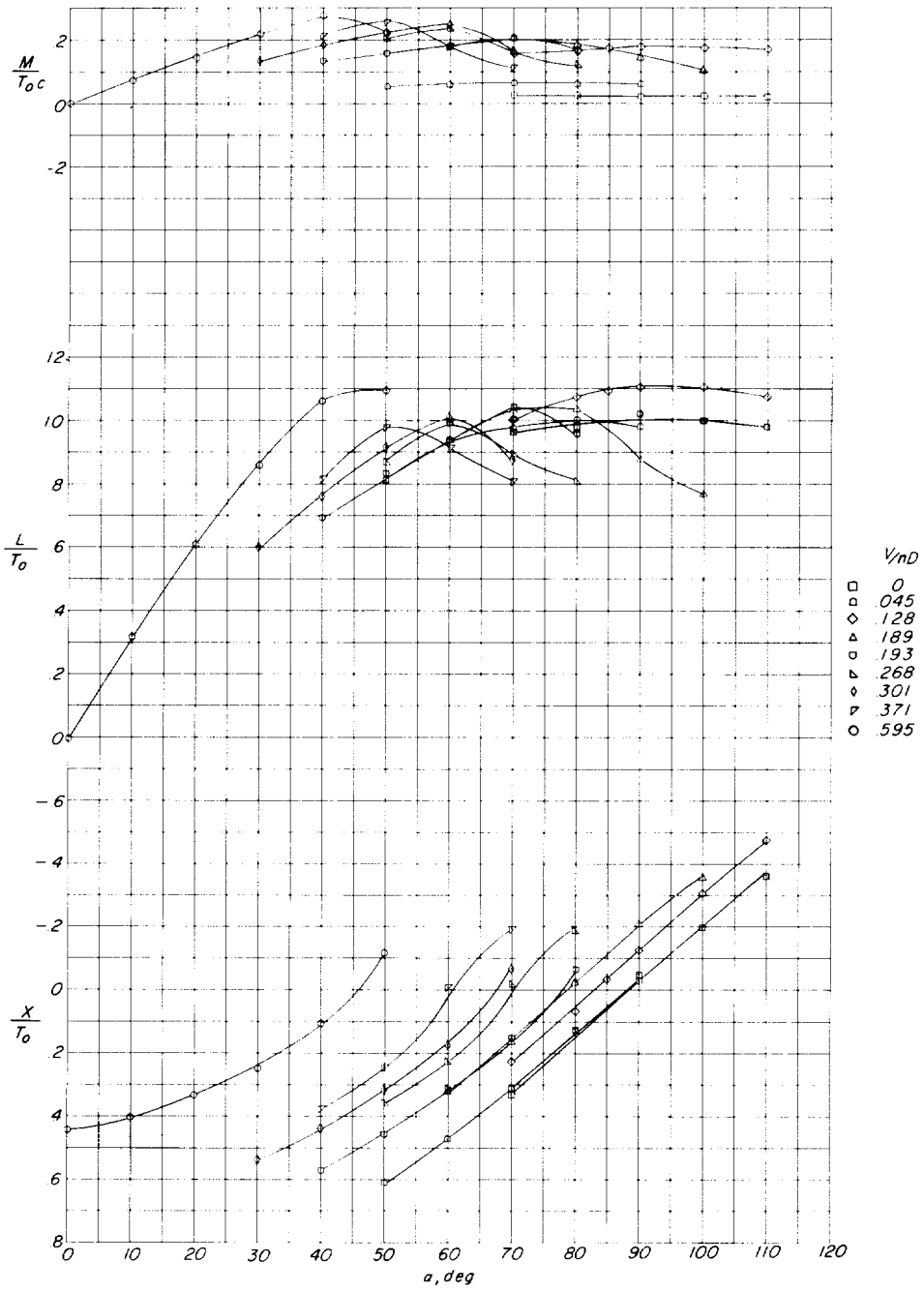

(a) Lift, longitudinal force, and pitching moment (original-lip configuration).

Figure 9.- Effect of advance ratio and angle of attack on the aerodynamic characteristics of the original-lip configuration.

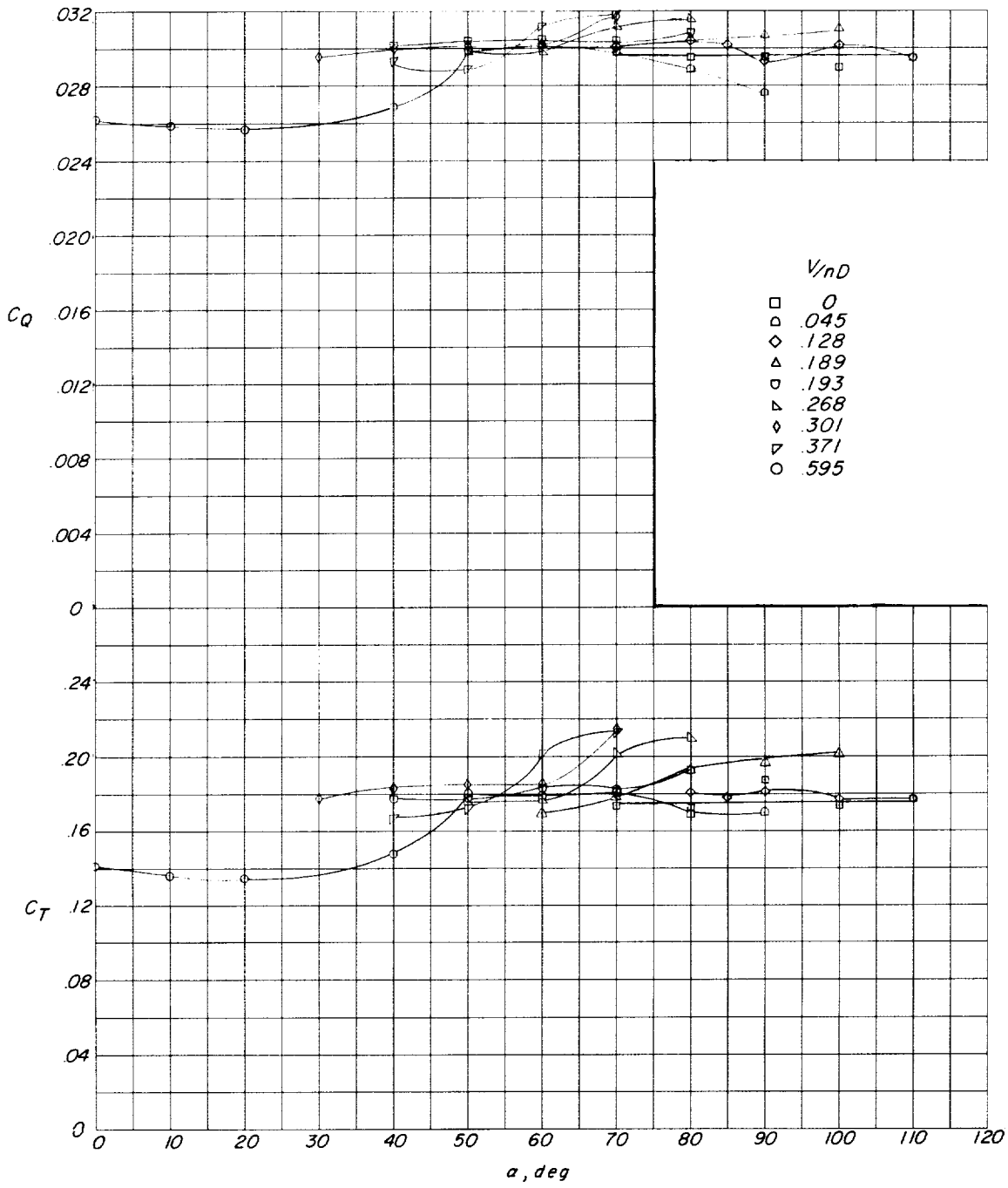

(b) Propeller thrust and torque coefficients (original-lip configuration).

Figure 9.- Continued.

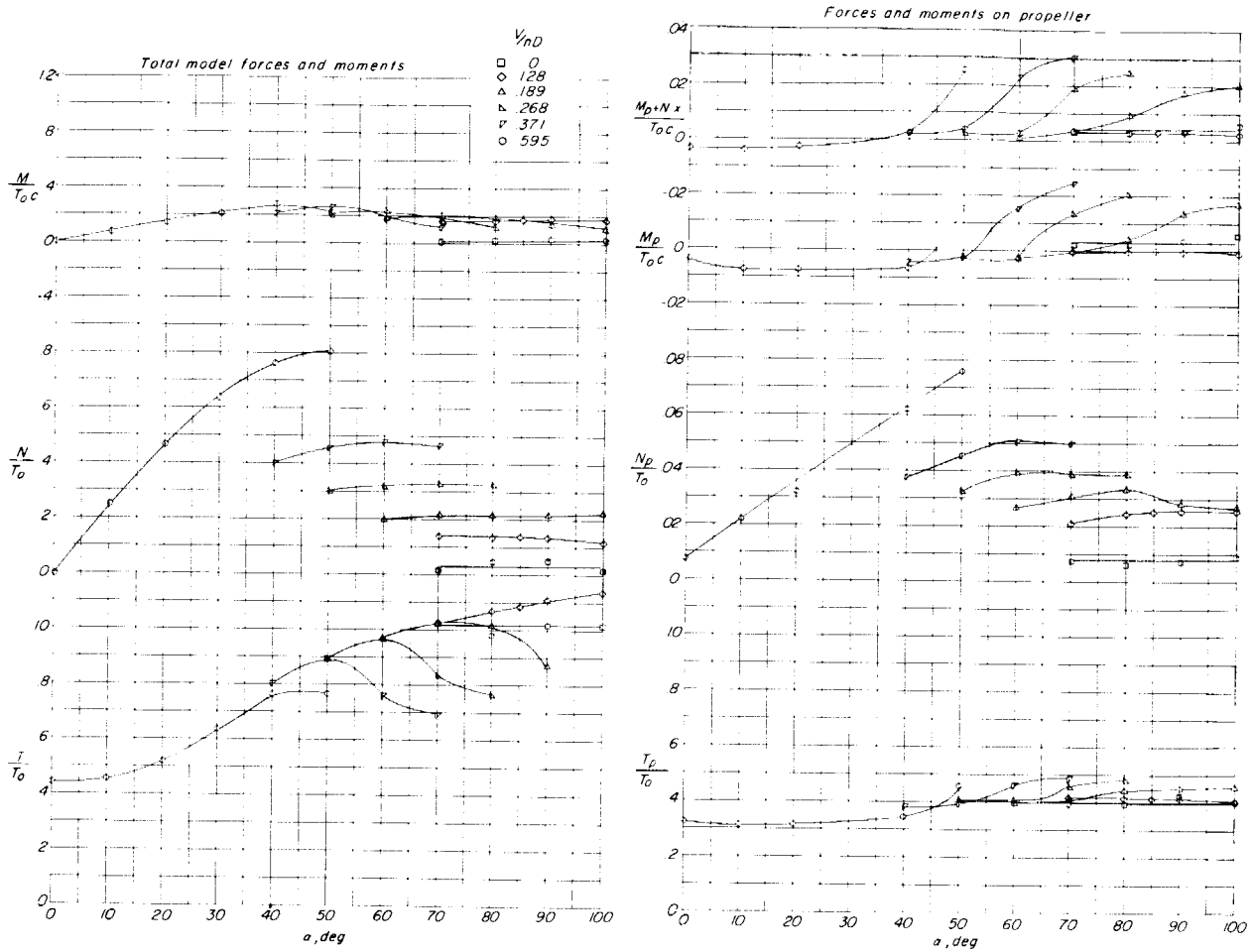

(c) Comparison of forces and moments on the propeller with the total model forces (original-lip configuration).

Figure 9.- Concluded.

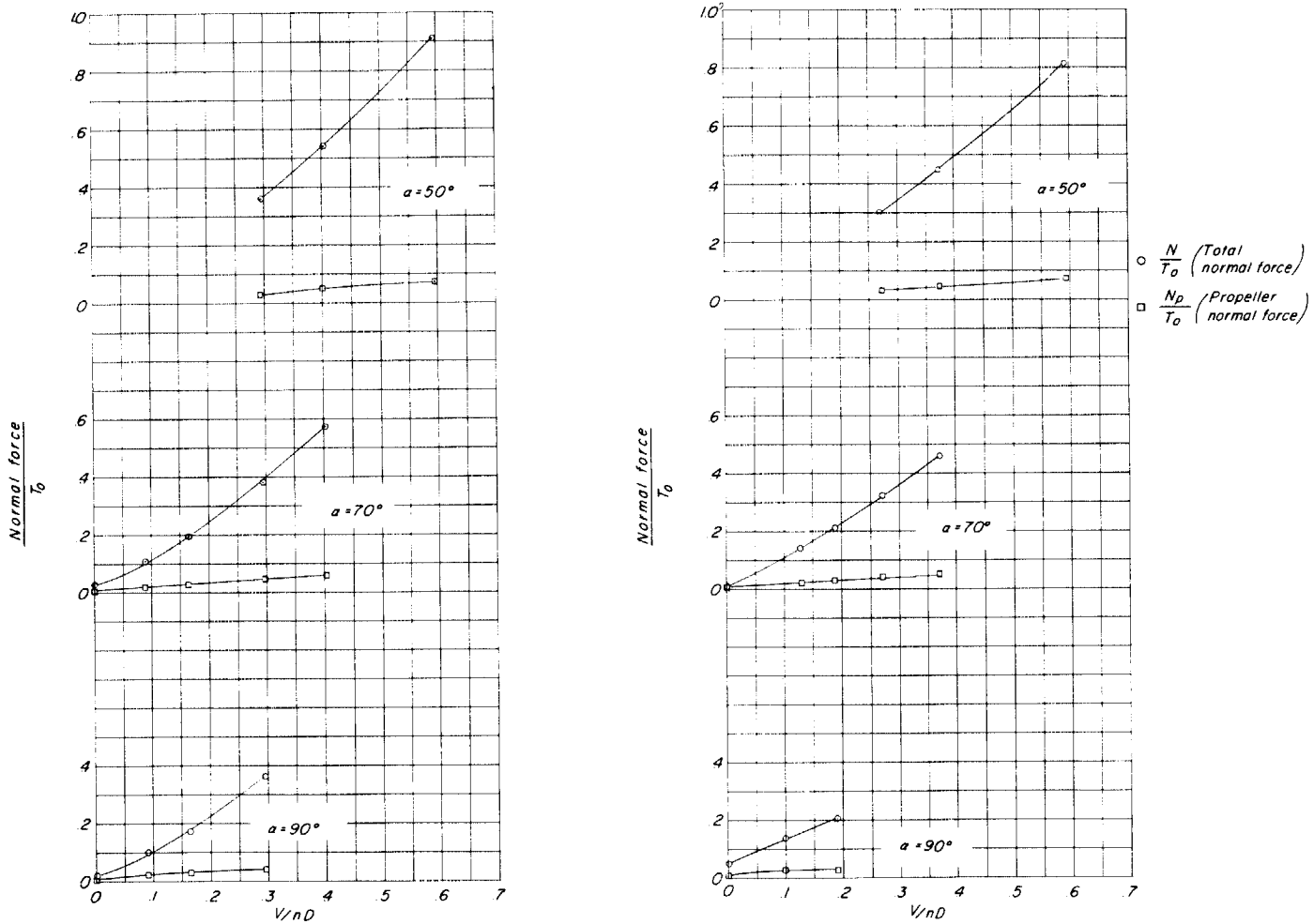

(a) Modified-lip configuration.

(b) Original-lip configuration.

Figure 10.- Comparison of the propeller normal force with the total normal force.

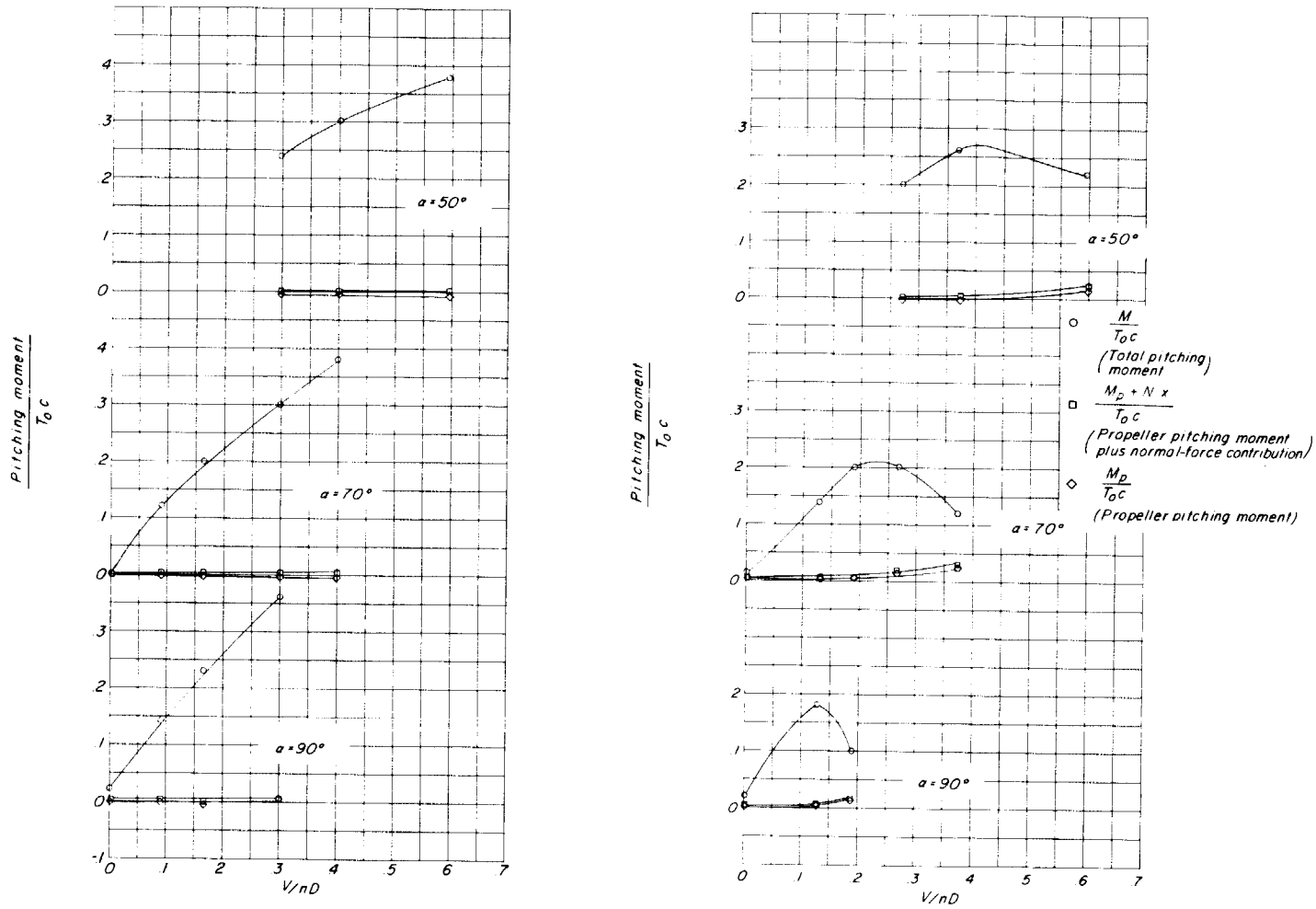

(a) Modified-lip configuration.

(b) Original-lip configuration.

Figure 11.- Comparison of propeller pitching moment with total pitching moment.

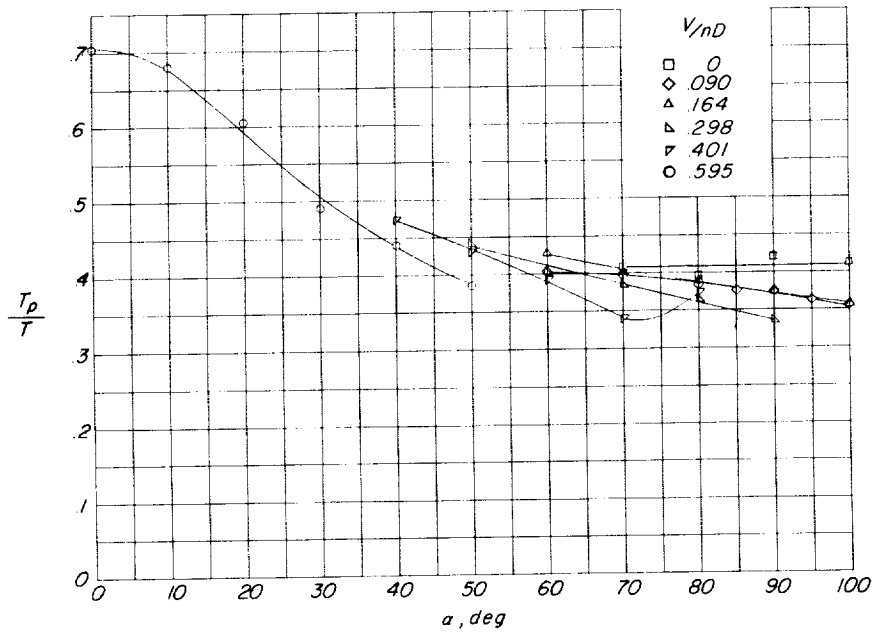

(a) Modified-lip configuration.

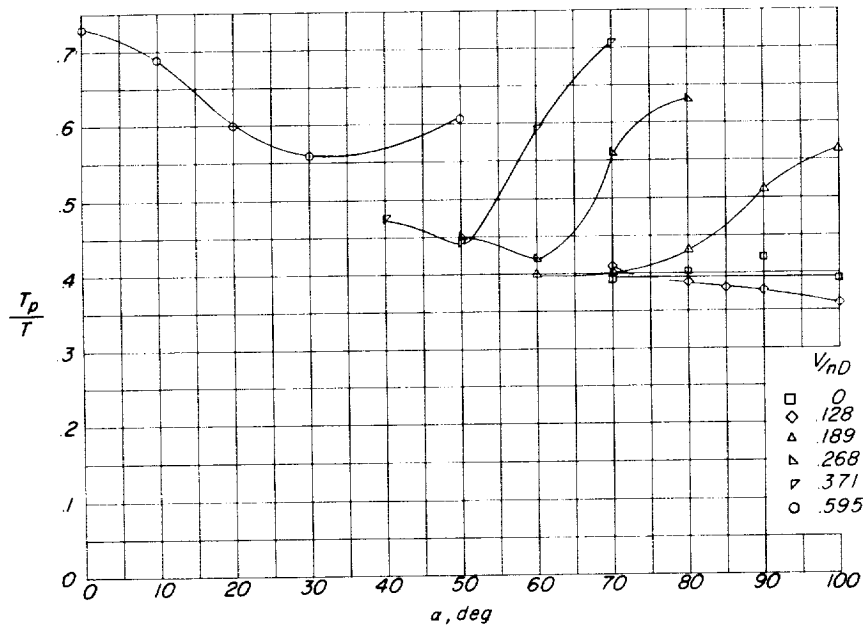

(b) Original-lip configuration.

Figure 12.- Variation of the ratio of propeller thrust to total thrust with angle of attack.

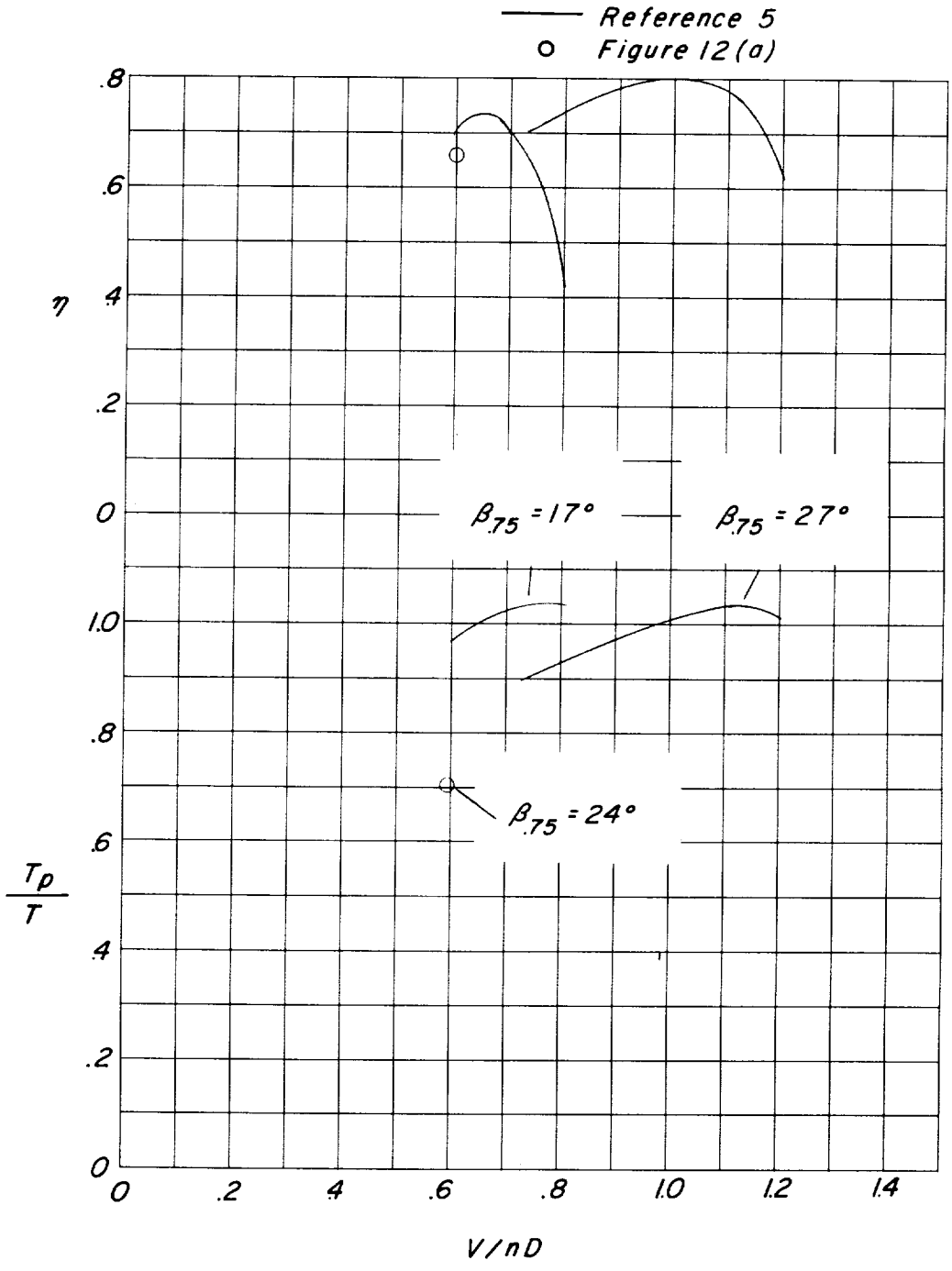

Figure 13.- Propulsive efficiency and ratio of propeller thrust to total thrust for modified configuration and configuration tested in reference 5. $\alpha = 0^{\circ}$.